

## Mechanical behavior of gas-saturated methane hydrate-bearing sediments

Masayuki Hyodo,<sup>1</sup> Yanghui Li,<sup>1,2</sup> Jun Yoneda,<sup>3</sup> Yukio Nakata,<sup>1</sup> Norimasa Yoshimoto,<sup>1</sup> Akira Nishimura,<sup>1</sup> and Yongchen Song<sup>2</sup>

Received 26 April 2013; revised 22 September 2013; accepted 4 October 2013; published 23 October 2013.

[1] A series of triaxial compression tests were conducted in order to investigate the mechanical behavior of gas-saturated methane hydrate-bearing sediments, and a comparison was made between gas-saturated and water-saturated specimens. Measurements on gas-saturated specimens indicate that (1) the larger the methane hydrate saturation, the larger the failure strength and the more apparent the shear dilation behavior; (2) failure strength and stiffness increase with increasing effective confining stress and pore pressure applied during compression, though the specimen becomes less dilative under higher effective confining stress; (3) lower temperatures lead to an increase of the stiffness and failure strength; (4) stiffness of specimens formed under lower pore pressure is higher than that of specimens formed under higher pore pressure but at the same effective stress; (5) stiffness and failure strength of gas-saturated specimens are higher than those of water-saturated specimens; (6) gas-saturated specimens show more apparent strain-softening behavior and larger volumetric strain than that of water-saturated specimens.

**Citation:** Hyodo, M., Y. Li, J. Yoneda, Y. Nakata, N. Yoshimoto, A. Nishimura, and Y. Song (2013), Mechanical behavior of gas-saturated methane hydrate-bearing sediments, *J. Geophys. Res. Solid Earth*, 118, 5185–5194, doi:10.1002/2013JB010233.

### 1. Introduction

[2] Methane hydrate, a crystalline material made up of a water cage surrounding a methane molecule [Sloan, 1998, 2003], forms naturally in regions of permafrost and continental margin sediment where there are appropriate pressure/temperature conditions and sufficient methane gas [Dawe and Thomas, 2007; Milkov, 2004]. A conservative estimate for the global gas hydrate inventory is  $\sim 1.8 \times 10^3$  Gt carbon, corresponding to  $\text{CH}_4$  volume of  $\sim 3.0 \times 10^{15}$  m<sup>3</sup> if the  $\text{CH}_4$  density is taken as 0.717 kg/m<sup>3</sup> [Boswell and Collett, 2011]. Such large amounts of carbon have prompted methane hydrate to be considered a potential energy resource, a geohazard, and a climate change agent [Boswell, 2009; Brown *et al.*, 2006; Dawe and Thomas, 2007; Glasby, 2003]. During the production of methane from hydrates, hydrate dissociation may induce a variety of geological disasters, such as subsea landslides, casing deformation, and production platform collapse [Ning *et al.*, 2012; Rutqvist *et al.*, 2009]. Thus, it is important to study the mechanical

properties of methane hydrate-bearing sediments for safe extraction of methane from hydrate reservoirs.

[3] A series of experimental studies on the mechanical properties of hydrate-bearing sediments have been conducted. Yun *et al.* [2007] studied the mechanical properties of sand, silt, and clay containing tetrahydrofuran (THF) hydrate. However, as THF hydrate forms without a gas phase and has a different structure than methane hydrate [Waite *et al.*, 2009], the applicability of results from THF hydrate experiments to natural hydrate deposits still needs to be discussed [Lee *et al.*, 2007]. Hyodo *et al.* [2005, 2011, 2013] performed a series of triaxial compression tests on Toyoura sand containing methane hydrate under similar conditions to those found in situ and obtained relationships among shear strength, temperature, pore pressure, and hydrate saturation. They also conducted plane strain shear tests to study the localized deformation of methane hydrate-bearing sand [Yoneda *et al.*, 2011]. Masui *et al.* [2005, 2008] studied the mechanical characteristics of both natural and artificial gas hydrate-bearing sediments. Constitutive models describing the stress-strain behavior for methane hydrate-bearing sediments were established [Uchida *et al.*, 2012; Yoneda *et al.*, 2008]. These studies all utilized water-saturated specimens.

[4] The mechanical properties of gas-saturated sediments containing methane hydrate are also of importance. Specimens with excess methane gas are analogs for natural gas-rich systems such as those that may occur when gas recycles into an upward-migrating base of hydrate stability [Waite *et al.*, 2004, 2008], as inferred by some for the Cascadia margin [Yuan *et al.*, 1999] and Blake Ridge [Guerin *et al.*, 1999]. Gas hydrates may also have formed from free gas in permafrost

<sup>1</sup>Department of Civil and Environmental Engineering, Yamaguchi University, Ube, Japan.

<sup>2</sup>Key Laboratory of Ocean Energy Utilization and Energy Conservation of Ministry of Education, Dalian University of Technology, Dalian, China.

<sup>3</sup>National Institute of Advanced Industrial Science and Technology, Tsukuba, Japan.

Corresponding author: Y. Li, School of Energy and Power Engineering, Dalian University of Technology, Dalian, Liaoning 116024, China. (li.yanghui@mail.dlut.edu.cn)

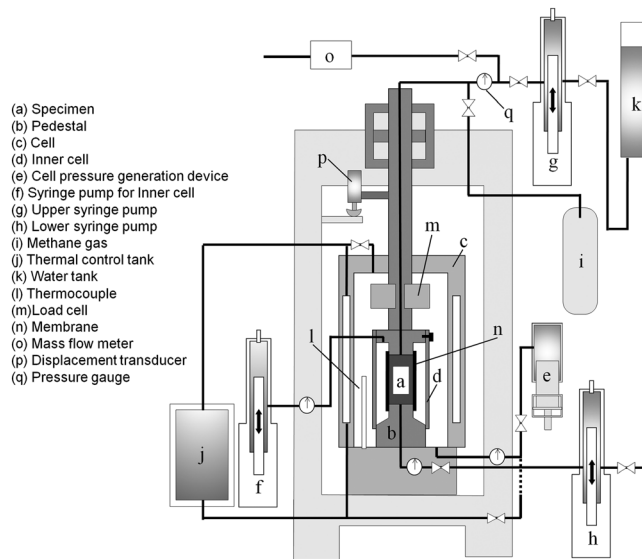


**Figure 1.** Schematic diagram of temperature-controlled high-pressure triaxial testing apparatus.

regions as cooler temperatures propagated into the sediment, and existing free gas was consumed to form hydrate [Collett *et al.*, 2011].

[5] Waite *et al.* [2004] formed methane hydrate in partially water-saturated Ottawa sand samples containing an interconnected methane gas phase. The results suggested that methane hydrate cements unconsolidated sediment when forming in systems containing an abundant gas phase. Also, the physical and mechanical properties are different than when methane hydrate forms in a water-rich system without an abundant free-gas phase. Priest *et al.* [2009] studied the influence of gas hydrate morphology on the seismic velocities of sands and provided a nice example of how velocities are significantly higher in hydrate-bearing sands formed with excess gas than with excess water. Ebinuma *et al.* [2005] studied the influence of pore fluid on the mechanical properties of hydrate-bearing sediments and indicated that the strength of gas-saturated hydrate specimens is stronger than that of water-saturated hydrate specimens. Li *et al.* [2011, 2012a, 2012b, 2012c, 2013] primarily studied the effect of temperature, confining pressure, strain rate, and porosity on the mechanical properties of synthetic methane hydrate and clayey sediment containing methane hydrate under subzero conditions. The specimens were gas saturated but contained ice powders. The mechanical behavior of gas-saturated methane hydrate-bearing sediments is not well understood, and further investigations should be carried out.

[6] In this paper, a series of tests were conducted in order to investigate the mechanical behavior of gas-saturated methane hydrate-bearing sediments which formed in partially water-saturated Toyoura sand under various conditions. An innovative temperature-controlled high-pressure triaxial apparatus which can reproduce the in situ conditions of a hydrate reservoir was used.

## 2. Experiment

### 2.1. Experimental Apparatus

[7] A temperature-controlled high-pressure triaxial testing apparatus was developed to simulate the in situ conditions

of methane hydrate reservoirs in the deep seabed. The schematic diagram of the apparatus is shown in Figure 1. A detailed description of this apparatus can be found in our earlier studies [Hyodo *et al.*, 2013].

[8] The apparatus can simulate in situ pressure ( $P$ ), temperature ( $T$ ), and stress conditions in a cylindrical sample, which is typically 30 mm in diameter by 60 mm in height. A sample covered with butyl rubber membrane is settled on the pedestal and then triaxial compression tests can be conducted in a temperature range from  $-35^{\circ}\text{C}$  to  $50^{\circ}\text{C}$  with axial load capacity of 200 kN, cell pressure capacity of 30 MPa, and pore pressure capacity of 20 MPa. A cell pressure generation device is used to maintain the confining pressure surrounding the sample. Two syringe pumps are used to control the pore pressure in the sample. A thermal control tank is used to adjust the temperature of the sample with an accuracy of  $\pm 0.1^{\circ}\text{C}$  by circulating the cell fluid in the triaxial testing device. A thermocouple placed near the side of the sample is used to measure the sample temperature.

[9] For water-saturated samples, methane hydrate saturation is calculated from the dissociated methane gas volume which is measured with a gas flowmeter. The residual methane gas

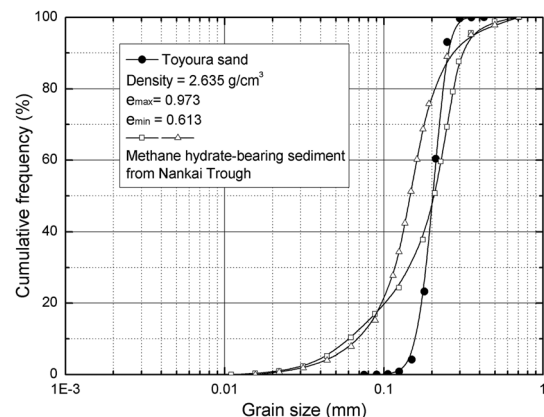


**Figure 2.** Grain size distribution of natural cores and Toyoura sand.

**Table 1.** Test Conditions of Triaxial Compression Tests<sup>a</sup>

$\sigma_c'$ (MPa)	Test Condition					Remarks $q_{max}$ (MPa)
	$P.P.$ (MPa)	$T$ (°C.)	$F.P.$ (MPa)	$S_{mh}$ (%)	$n$ (%)	
1	5	5	0	0	39.3	3.25
			4	43.6	39.7	6.99
3	5	5	0	0	39.4	6.97
			4	23.4	39.4	10.17
			4	42.5	40.7	11.30
	10	1	4	23.2	38.7	14.31
			4	26.6	39.0	10.57
		5	12	24.7	39.0	9.20
			12	47.7	39.5	16.46
12	5	12	23.2	39.5	11.73	

<sup>a</sup>The  $\sigma_c'$  is effective confining stress;  $P.P.$  is the pore pressure applied during compression;  $F.P.$  is the pore pressure applied during hydrate formation;  $S_{mh}$  is methane hydrate saturation;  $n$  is porosity;  $q_{max}$  is the maximum deviator stress (failure strength).

will be drained out by pushing water through the specimen. The volume change of the specimens during the shear process is measured by the drained pore water, which is collected by the two syringe pumps.

[10] For gas-saturated samples, methane hydrate saturation is calculated from the initial water content of the samples. The volume change of gas-saturated samples cannot be measured by the drained pore water in the usual way, so a double-cell design is adopted. The volume change of gas-saturated specimens equals the volume change of the inner cell minus the volume of drained fluid from the inner cell, which can be obtained by measuring the volume difference of the syringe pump for the inner cell and the displacement of the piston.

## 2.2. Experimental Procedure and Test Conditions

[11] Based on the observation of the undisturbed core samples obtained from Nankai Trough [Masui *et al.*, 2008; Suzuki *et al.*, 2009], Toyoura sand was chosen as the host material for this study. The grain size distributions of the natural cores and Toyoura sand are shown in Figure 2. The relative density ( $Dr = \frac{e_{max} - e}{e_{max} - e_{min}}$ ) of each host sample was approximately 90%, indicating that the sand particles in the host sample were well compacted. The porosity of each host sample was about 39%–41%.

[12] Methane hydrate-bearing sediments formed from partially water-saturated Toyoura sands were prepared by the following procedure: first, moist sand with a determined initial water content was put into a specimen mold (30 mm in diameter and 60 mm in height) in 15 layers and each layer was compacted with a tamper 40 times. Extra water (0.14 g) was used to consider the water evaporation for each specimen. Then, the mold filled with moist sand was placed in a freezer (about  $-20^\circ\text{C}$ ) to make the sample stand by itself. Next, the frozen specimen was taken out from the mold and placed on the pedestal, and the butyl rubber membrane was put into place.

[13] Methane gas was injected into the sample and gradually increased to the desired pore pressure for hydrate formation ( $F.P.$ ) (see Table 1) while the cell pressure was continuously kept 0.2 MPa higher than pore pressure. Then, the temperature was turned to  $1^\circ\text{C}$  while keeping the pore gas pressure constant. These conditions were kept constant

for 24 h to generate methane hydrate. We considered that the water was fully converted to hydrate when there was no obvious volume change in the upper and lower syringe pumps connected to the top and bottom of the specimen. The methane hydrate saturation was calculated from the initial water content. According to the study of Circone *et al.* [2005], a ratio of  $\sim 6.0$   $\text{H}_2\text{O}$  per mole of  $\text{CH}_4$  was used to calculate the saturation. A volume increase of  $\sim 15\%$  occurred when the ice converted to hydrate, but the expanded volume would fill into the empty pores during hydrate formation with little volume change of samples. In this study, the volume change of samples during the formation of hydrate was ignored. After hydrate formation was completed, the desired pore pressure was applied by injecting methane gas through the two syringe pumps. Cell pressure and temperature were adjusted to the desired condition (Table 1). Next, isotropic consolidation was carried out until the specified stress was reached and then shear tests were conducted. The axial strain rate was 0.1%/min.

[14] All hydrate-bearing specimens were prepared as described above. To obtain a water-saturated hydrate-bearing specimen, the specimen was water flooded after the hydrate formation step: Pure water from the lower syringe pump was injected through the specimen base to replace the gaseous methane remaining in the pores of the specimen, pedestal, and pipework. During this water substitution process, cell pressure, pore pressure, and temperature were kept constant. The Toyoura sand and hydrate-free specimens used in this work were all water-saturated.

[15] In this work, the effective confining stress is the difference between the pore pressure and cell pressure. The deviator stress is defined as the stress after subtracting the effective confining stress from the axial stress. The axial strain is calculated by dividing the axial displacement by the height of the specimen after consolidation but prior to shear. The volumetric strain is given by the volume change divided by the volume of the specimen after consolidation but prior to shear. A positive strain value denotes compression. Strain hardening is defined as the region in which a material is deformed in order to increase its resistance to further deformation. Strain softening is defined as the region in which the stress in the material is actually decreasing with an increase in strain. The stiffness is a measure of the resistance offered

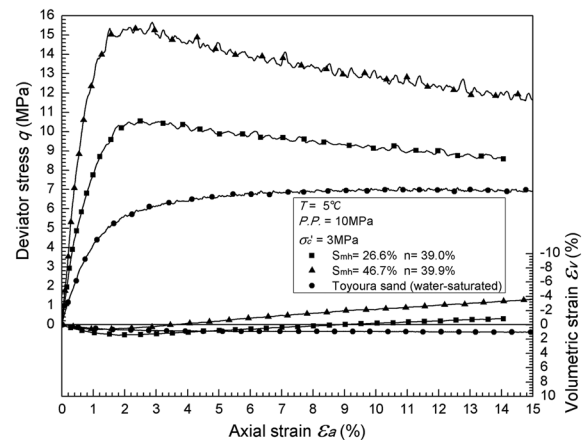


**Figure 3.** The influence of methane hydrate saturation,  $S_{mh}$ , given a 10 MPa pore pressure.

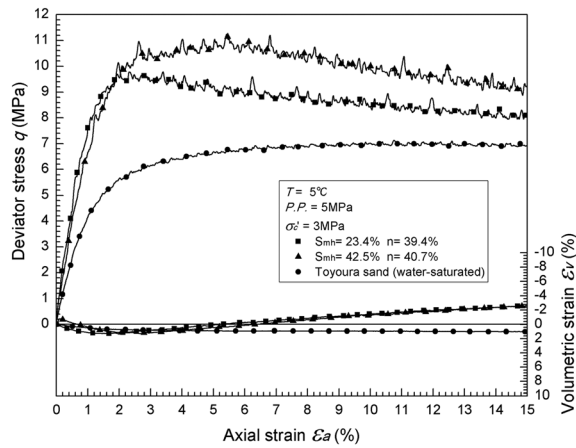


**Figure 4.** The influence of methane hydrate saturation,  $S_{mh}$ , given a 5 MPa pore pressure.

by the material to deformation and can be represented by the slope of its stress-strain curve.

### 3. Results and Discussion

#### 3.1. Effect of Methane Hydrate Saturation

[16] Figures 3 and 4, respectively, show the deviator stress and volumetric strain dependence on axial strain for gas-saturated methane hydrate-bearing specimens having pore pressures of 10 MPa (Figure 3) or 5 MPa (Figure 4).

[17] In the case of water-saturated sand specimens ( $S_{mh} = 0\%$ ), the deviator stress increased gradually with increasing axial strain and finally reached a constant value with a reasonably asymptotic behavior until axial strain reached 15%. A significant strain-hardening behavior and shear contraction were shown during the shear tests.

[18] Sand particles are displaced and can be crushed during the shear tests. Specimen contraction can occur as existing pore space fills with the fine particles or the crushed sand particles. When the specimen is sheared beyond a certain void ratio, however, some part of the sand particles has to roll across the others, resulting in specimen dilation. As is observed in Figures 3 and 4, the volumetric strain initially showed a positive compression and then remained almost constant during the latter half of the test. This suggests the pore-filling contractive effect and the rolling effect offset each other or the critical state of the specimen was reached at the end of the shear test. The critical state concept states that soils and other granular materials, if continuously sheared until they flow as a frictional fluid, will come into a well-defined critical state. In the absence of hydrate, *Yun et al.* [2007] considered that shear would cause particle rotation, slippage, and rearrangement. The rotation frustration in densely packed sediments (which we used in this work) is overcome by either dilation (low confinement) or slippage (high confinement). The mechanism by which the sample deforms at a micromechanical level is governed by the energy minimization principle.

[19] In the case of methane hydrate-bearing specimens, a strain-softening behavior and shear dilation were observed during the shear tests. The deviator stress increased until it reached a peak value at axial strain of 1%–3% and then the deviator stress gradually decreased. The volumetric strain

shows shear contraction at the beginning of the shear test, and significant dilative behavior was observed at the end of the shear tests.

[20] Methane hydrates occupy the pore space of the specimen, and there is not sufficient pore space that can be filled in during the compression. Sand particles have to roll across each other, which leads to dilation of the specimens as shown in Figures 3 and 4. When the sand particles pass by each other, the specimen becomes loose, causing a decline of strength. Also, the cementation is gradually destroyed with increasing axial strain/deformation, which causes a decline of strength. Both processes cause strain-softening behavior. *Yun et al.* [2007] suggested that hydrate-occupied porosity governs deformation and strength response, and hydrate crystals may shear, may detach from the mineral surface, or may interfere with rotation. The impact of these mechanisms on dilation and strength depends on the strength, bonding strength, and concentration of hydrate. The presence of hydrate would enhance dilation.

[21] *Miyazaki et al.* [2011] studied the mechanical properties of water-saturated methane hydrate-bearing sediments using Toyoura sand as a host material. The specimens also showed strain-softening behavior starting around an axial strain of ~3%, and the failure strength increased with increasing methane hydrate saturation. However, the observations on the water-saturated methane hydrate-bearing sediments by *Hyodo et al.* [2013] differ from those of *Miyazaki et al.* [2011], which showed strain softening starting at a much later strain. *Hyodo et al.* [2013] observed a strain-hardening behavior before the axial strain reached 15%, and the declination of strength did not occur until the axial strain exceeded 20%.

[22] These differences may be caused by the formation conditions of methane hydrate-bearing sediments. *Miyazaki et al.* [2011] formed methane hydrate under the desired initial shear-testing conditions, meaning that the particles will be rearranged to be more dense due to the high effective stress prior to the formation of hydrate. *Hyodo et al.* [2013] formed methane hydrate under low-effective stress (0.2 MPa) prior to consolidating the specimen to the initial shear-testing conditions. Once hydrate forms, the cementation effect can resist the deformation of the specimen and drainage of pore water during consolidation. This allows the specimen to remain

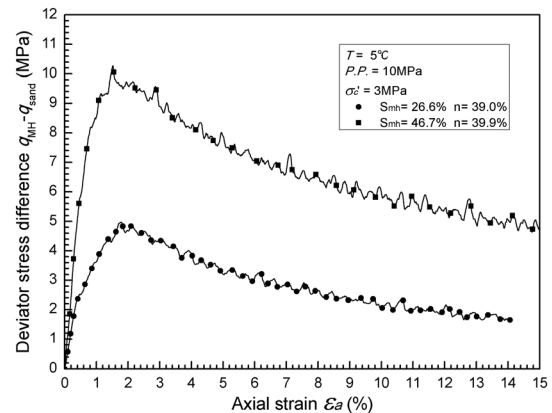


**Figure 5.** The deviator stress difference relative to host Toyoura sand depends strongly on methane hydrate saturation.

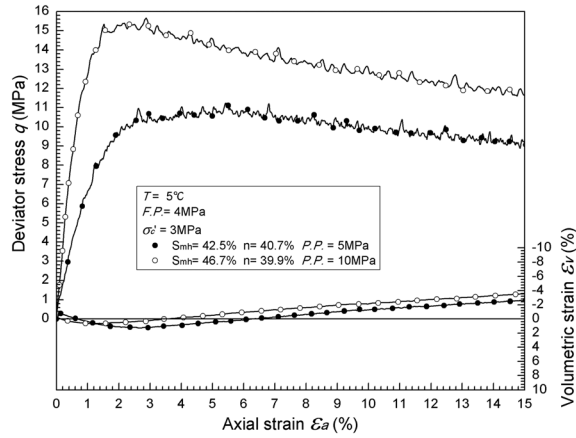


**Figure 6.** The deviator and volumetric strain dependence on the pore pressure applied during compression for specimens formed at 4 MPa pore pressure.

looser than that of specimens containing hydrate formed after consolidation. Also, the porosity should be considered: The specimens *Miyazaki et al.* [2011] used are 37.8%, which is smaller than that of *Hyodo et al.* [2013] used. Strain softening occurs more easily in dense specimens due to the movement of sand particles as clarified above.

[23] The mechanical properties of gas-saturated methane hydrate-bearing sediments varied with the methane hydrate saturation: The larger the methane hydrate saturation, the larger the strength (maximum deviator stress during the test) and the more apparent the shear dilation behavior, while in Figure 4, both hydrate specimens showed the same volumetric strain response. It is because of this that the specimen with higher saturation (42.5%) has a larger porosity than that of the specimen with hydrate saturation of 23.4%, which may lead to less dilation during shear.

[24] Hydrates formed from excess gas cement grains [*Priest et al.*, 2009; *Waite et al.*, 2004], and the cementation increases with increasing methane hydrate saturation. Bulk density also increases with increasing methane hydrate saturation, which enhances the strength. The void ratio decreases due to the increase of methane hydrate saturation, which leads to a more apparent dilative behavior.

[25] Figure 5 shows the deviator stress difference relative to water-saturated, hydrate-free Toyoura sand for methane hydrate saturations of 26.6 and 46.7%, an effective confining stress of 3 MPa, pore pressure of 10 MPa, and temperature of 5°C. It can be observed that the deviator stress difference increased almost linearly at the beginning of the test and then decreased after it reached a peak value at the axial strain 1%–3%. The deviator stress increment increased with increasing methane hydrate saturation, but the following decline of the deviator stress increment was almost the same under both methane hydrate saturations. It is believed that the strength increment increases with increasing cementation of the sediment grains by hydrate and with the increasing bulk density of the specimen. Methane hydrate cements grain contacts, which may restrict the rotation and slide of the grains, enhance the resistance of deformation, and increase the failure strength. This cement contact breaks down with increasing deformation, causing a decline of strength increment as shown in Figure 5. The broken hydrates act as host

particles in the pore space. Sand particles and hydrate particles roll across the others, resulting in specimen dilation as mentioned above.

[26] In the case of water-saturated methane hydrate-bearing sediments, the strain-softening behavior is affected by methane hydrate saturation: the larger the methane hydrate saturation, the more apparent the strain-softening behavior [*Miyazaki et al.*, 2011], which is not observed in our study. It is considered that the pore water/gas cannot be drained out easily during shear due to the low permeability of the specimen. And the pore pressure increases in some blocked regions, which leads to a decrease of effective confining stress during shear, and then weakens the strength (softening behavior). The permeability decreases with increasing hydrate saturation, and the pore pressure of higher hydrate saturation specimens will increase more during shear. However, considering the high compressibility of methane gas, the pore pressure of gas-saturated specimens will not change a lot during shear, and thus, the softening behavior changes a little with increasing hydrate saturation.

### 3.2. Effect of Pore Pressure

[27] Figures 6 and 7 show the deviator stress and volumetric strain plotted against the axial strain for the gas-saturated methane hydrate-bearing specimens under several pore pressures (the pore pressure applied during compression). For a given methane hydrate saturation, formation pressure, and effective confining stress, the deviator stress and stiffness clearly depended on the pore pressure; under higher pore pressures, the specimen had a larger strength and stiffness (Figure 6). While in Figure 7, there was a 20% increase in pore pressure between the specimens and the stress-strain curves overlaid each other prior to failure, meaning there was no difference in stiffness. It is considered that the stiffness is also affected by hydrate saturation and bulk density. In Figure 7, the specimen under higher pore pressure (12 MPa) had lower hydrate saturation and larger porosity than those of the specimen under 10 MPa pore pressure, which may decrease the stiffness of the specimen.

[28] *Hyodo et al.* [2013] showed a similar result on water-saturated methane hydrate-bearing specimens, but *Miyazaki et al.* [2011] suggested that the water-saturated methane

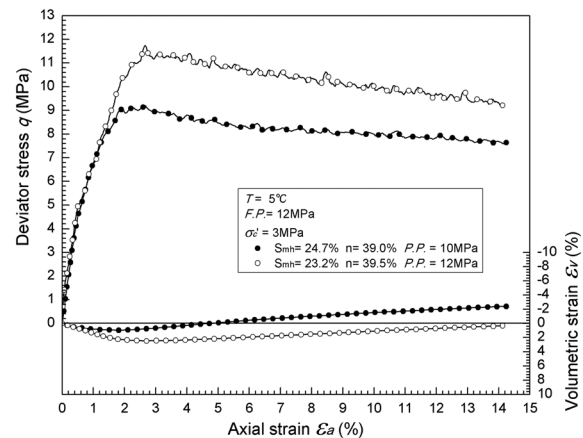


**Figure 7.** The deviator and volumetric strain dependence on pore pressure for specimens formed at 12 MPa pore pressure.

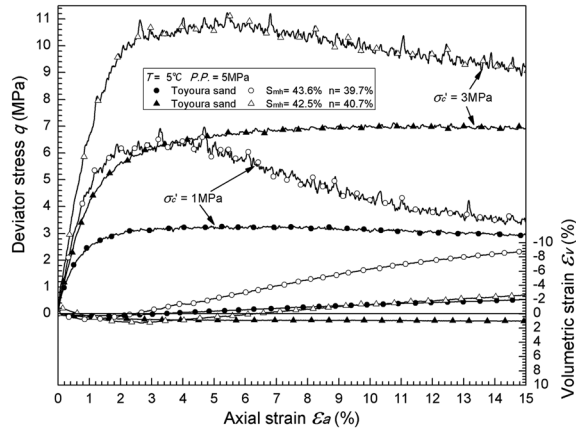


**Figure 8.** The influence of effective confining pressure on the mechanical behavior of gas-saturated hydrate-bearing specimens at 5 MPa pore pressure.

hydrate-bearing specimens with the same methane hydrate saturation had a similar strength under the same effective confining pressure, even when they had a different pore pressure.

[29] From Figures 6 and 7, it can be observed that the specimens showed the opposite effect on the volumetric strain with respect to pore pressure. The effect of pore pressure on the volumetric strain cannot be easily obtained in this paper. It is considered that higher dilation occurs when the specimen has more hydrate and smaller porosity.

[30] In hydrate-bearing specimens, some pores will be blocked by hydrate cement at grain contacts. The gas may be isolated and unconnected in some local region in specimen. A blocked pore or cluster of pores with the surrounding sand particles and hydrate can be considered as an associative unit. Under higher pore pressure and a certain effective stress, this unit may experience plastic deformation and creep and be compacted. The samples become more dense, which results in the enhancement of strength.

**3.3. Effect of Effective Confining Stress**

[31] Gas-saturated methane hydrate-bearing specimens were subjected to different effective confining stresses, but

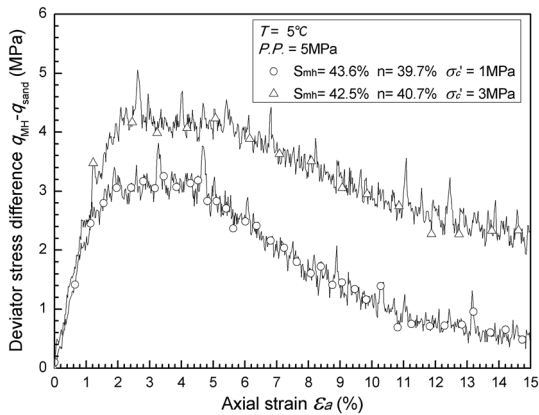


**Figure 9.** The deviator stress difference relative to host Toyoura sand dependence on effective confining pressures at 5 MPa pore pressure.

an identical pore pressure (B.P. = 5 MPa), temperature (5°C), and similar methane hydrate saturation ( $S_{mh} = 42\text{--}44\%$ ) were tested to examine the influence of the effective confining stress on the measured strength and deformation. The deviator stress, axial strain, and volumetric strain relationships for the specimens are shown in Figure 8. Both methane hydrate-bearing specimens under different effective confining stresses showed strain-softening behavior. The stiffness and failure strength of specimens containing methane hydrate were both higher than those of Toyoura sand and increased with increasing effective confining stress. A higher effective confining stress enhances the frictional force between the particles, and more energy is required to overcome the intergranular frictional force during the shear test.

[32] The volumetric strain exhibited less dilation with increasing effective confining stress at a given axial strain, indicating that the effective confining stress restrains the deformation of specimens. Higher effective confining stresses will increase the extent of sand particle breakage, and the crushed particles may move into the pore space during deformation, decreasing the dilation of the specimens.

[33] Figure 9 shows the deviator stress difference relative to the host Toyoura sand for 1 MPa and 3 MPa effective confining stresses for specimens with 42–44% methane hydrate saturation, a pore pressure of 5 MPa, and temperature of 5°C. It can be observed that the curves both increase until the peak value is reached at the axial strain 1–3% and then declined until the end. The incremental stress increase value of specimens under larger effective confining stress was higher than that of specimens under lower effective confining stress. It is considered that the rotation and slide of the sand particles are restricted under higher effective stress, which increases the difficulty of breaking the cementation between grain contacts. The strength decline due to the breakage of cementation and the strength enhancement due to rolling effect (the crushed hydrate acts as normal sand particles in the specimen) offset each other, which causes a flat region between 2 and 5% axial strain (Figure 9).

**3.4. Effect of Temperature**

[34] According to the literature, the strength of sand does not seem to depend on temperature [Graham *et al.*, 2004],

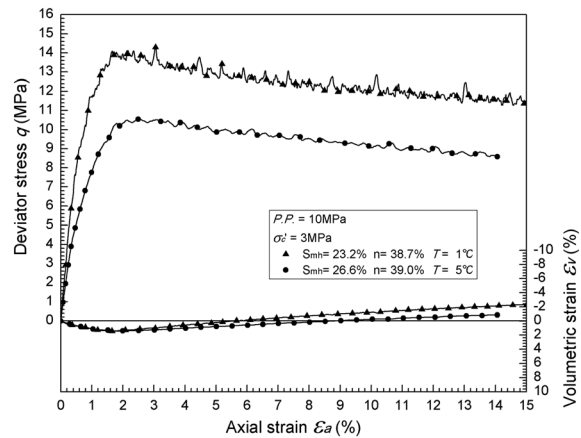


**Figure 10.** Strength decreased with increased temperature even though the sample at warmer temperatures had slightly more hydrate.

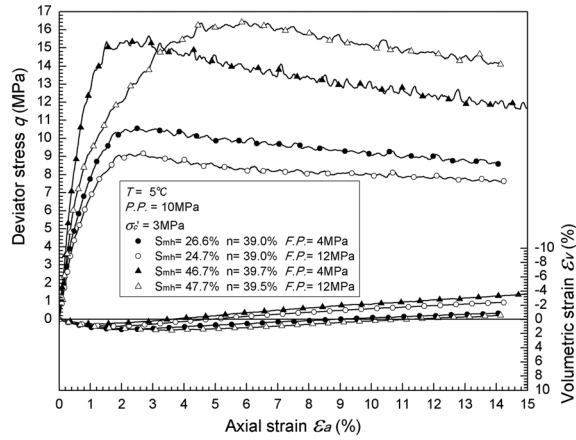


**Figure 11.** The influence of methane hydrate formation pressure on the mechanical behavior.

while the physical/chemical properties of gas hydrate are strongly affected by temperature [Sloan, 1998]. Helgerud et al. [2009] measured the compressional, P, and shear, S, wave speeds of pure gas hydrate, observing  $V_p$  and  $V_s$  decrease with increasing temperature. Yang et al. [2004] showed that particle-particle adherence forces in ice and clathrate hydrates were also functions of temperature. The measured forces decreased as the temperature was lowered from the freezing point of the particles.

[35] Figure 10 shows the temperature dependence of the mechanical properties of gas-saturated methane hydrate-bearing specimens. It can be observed that the stiffness and failure strength strongly depend on the magnitude of temperature. The temperature drop led to the increase of the stiffness and failure strength, in agreement with results from water-saturated methane hydrate-bearing sediments [Hyodo et al., 2013]. Durham et al. [2003] studied the strength and rheology of pure methane hydrate, which also showed the strength decreasing with increasing temperature. Their work suggests that the strength of hydrate-bearing sediments decreases at warmer temperatures due to the hydrate itself, though there may also be a contribution from a temperature dependence of the strength of the hydrate/sediment contact.

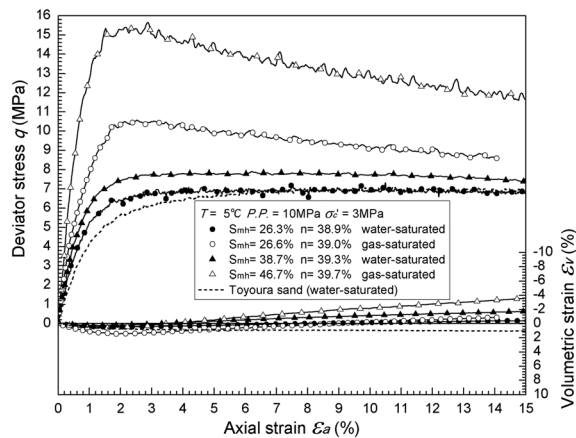


**Figure 12.** A comparison between the mechanical behavior of a gas-saturated specimen and water-saturated specimen under a pore pressure of 10 MPa, an effective confining pressure of 3 MPa, and a temperature of 5°C.

### 3.5. Effect of Formation Pressure

[36] Figure 11 shows the influence of methane hydrate formation pressure on the mechanical properties of gas-saturated methane hydrate-bearing specimens. The stiffness of specimens formed under lower pore pressure was higher than that of specimens formed under higher pore pressure. Failure strength and volumetric strain were also affected by the formation pressure, which should be investigated in more detail in our further studies.

### 3.6. Comparison With Water-Saturated Methane Hydrate Specimens

[37] A comparison between the deviator stress, axial strain, and volumetric strain relationships of gas-saturated specimens and water-saturated specimens [Hyodo et al., 2013] was made in this study. Figures 12 and 13 indicate the effects of pore fluid on the mechanical behavior of methane hydrate-bearing sediments. The stiffness and failure strength of gas-saturated specimens were higher than those of water-saturated specimens. In the water-saturated specimens, the deviator stress increased gradually with increasing axial strain and finally reached a constant value without any obvious peak value. A strain hardening was observed in these specimens. In the case of gas-saturated specimens, there was an apparent strain-softening behavior which was obviously different from that of water-saturated specimens. The volumetric strain of gas-saturated specimens was larger and more dilatative than that of water-saturated specimens. Similar results are also observed in the work of Ebinuma et al. [2005]. They suggested that the dependence of mechanical strength on the pore fluid is due to a decrease in the effective confining stress on the sand. The pore water will be suppressed, and thus, the pore pressure increases during shear due to the low permeability at high hydrate saturation. Priest et al. [2009] compared the wave velocity of a specimen formed by “excess gas” method with that of a specimen formed by the “excess water” method, and the excess gas specimen showed a higher strength (wave velocity) than did the excess water specimen. This agreement with our observations is in spite of the preparation of this excess water specimen being significantly different from water-saturated hydrate specimens used in our study.

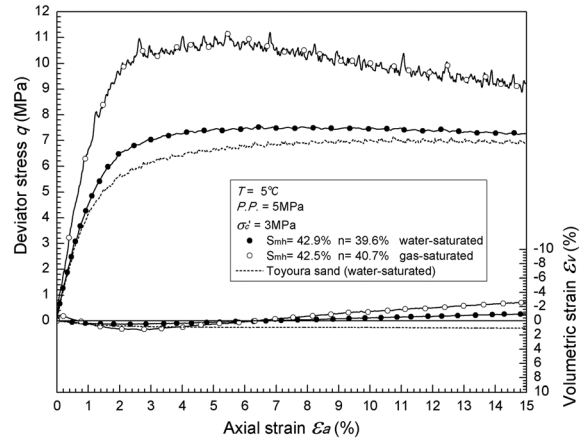


**Figure 13.** A comparison between the mechanical behavior of a gas-saturated specimen and water-saturated specimen under a pore pressure of 5 MPa, an effective confining pressure of 3 MPa, and a temperature of 5°C.

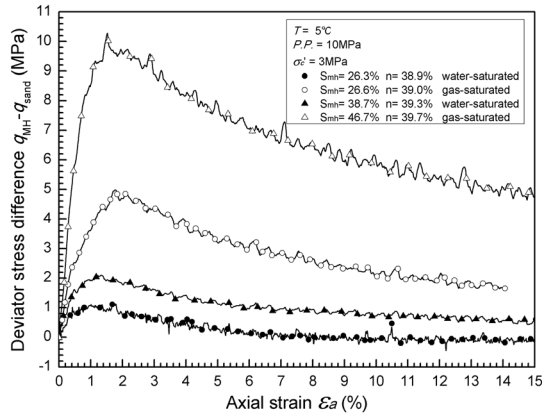


**Figure 14.** A comparison between the deviator stress difference relative to the host Toyoura sand for gas-saturated and water-saturated specimen under a pore pressure of 10 MPa, an effective confining pressure of 3 MPa, and a temperature of 5°C.

[38] Methane hydrate likely dissolves during the water saturation process, meaning the calculated methane hydrate saturation is higher than actual saturation of the specimen. Dissolving methane hydrate that had initially formed at sediment grains contacts would weaken the cementation effect between the hydrate and sand particles.

[39] Figures 14 and 15 show a comparison between the deviator stress difference relative to the water-saturated host Toyoura sand for gas-saturated and water-saturated methane hydrate-bearing specimens under various conditions. The peak deviator stress difference due to methane hydrate was observed in each case at axial strains of 1%–3%, regardless of the saturation condition. The deviator stress increment for gas-saturated specimens was larger than that of water-saturated specimens. After the peak value was reached, the deviator stress increment of gas-saturated specimens decreased more rapidly but the final residual deviator stress difference was still higher than that of water-saturated methane hydrate-bearing specimens.

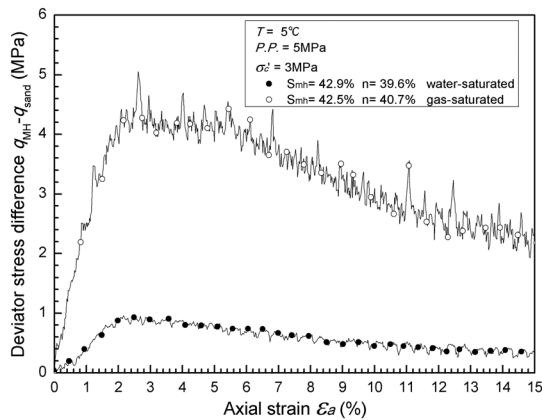


**Figure 15.** A comparison between the deviator stress difference relative to the host Toyoura sand for gas-saturated and water-saturated specimen under a pore pressure of 5 MPa, an effective confining pressure of 3 MPa, and a temperature of 5°C.

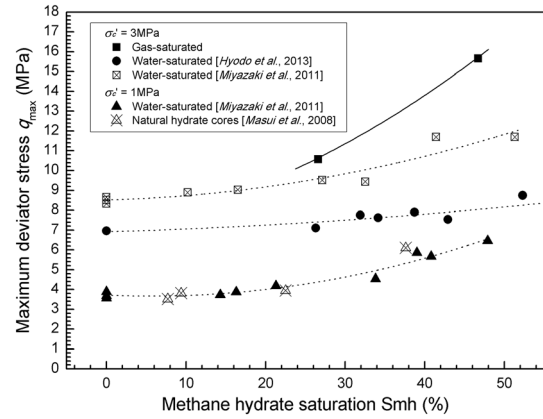


**Figure 16.** The maximum deviator stress of gas-saturated and water-saturated specimens plotted against the methane hydrate saturation.

[40] Figure 16 shows the maximum deviator stress plotted against the methane hydrate saturation under different saturation conditions. The failure strength of both gas-saturated and water-saturated specimens increased with increasing methane hydrate saturation. The failure strength of gas-saturated specimens showed a more marked dependency on methane hydrate saturation than water-saturated specimens. Also, note that the failure strength of water-saturated hydrate specimens used in the work of Miyazaki *et al.* [2011] is larger than that of Hyodo *et al.* [2013] due to the difference between applying the effective stress prior to hydrate formation [Miyazaki *et al.*, 2011] or after hydrate formation [Hyodo *et al.*, 2013], as discussed in section 3.1. In the study of Hyodo *et al.* [2013], a cylindrical-shaped load cell was set up inside the cell to eliminate the influence of piston friction which would be very large at high-cell pressures. Miyazaki *et al.* [2011] set up their load cell outside the cell and did not account for piston friction, so their strength results included the piston friction and showed larger values. The failure strength of water-saturated specimens shows the dependence on effective confining stress, which means it will also likely depend on burial depth in natural formations.

#### 4. Conclusions

[41] In this study, we conducted triaxial compression tests on laboratory-formed gas-saturated methane hydrate-bearing sediment samples to determine how the strength results depended on methane hydrate saturation, effective confining stress, temperature, and pore pressure applied during hydrate formation and during triaxial compression. A comparison was made between methane hydrate-bearing sediments that remained gas saturated and those that were water saturated following hydrate synthesis. On the basis of the obtained results, the findings can be summarized as follows:

- [42] 1. The mechanical properties of gas-saturated specimens vary with the methane hydrate saturation: The larger the methane hydrate saturation, the larger the failure strength and the more apparent the shear dilation behavior. Also, higher dilation occurs when the specimen has smaller porosity.
- [43] 2. The gas-saturated specimen has a larger failure strength and greater stiffness under higher effective confining stress and higher pore pressure applied during compression,

while the volumetric strain exhibits less dilation under higher effective confining stress. The effect of pore pressure applied during compression on the volumetric strain is still unclear in this study.

[44] 3. Lower temperatures lead to increased stiffness and failure strength of gas-saturated specimens.

[45] 4. The stiffness of gas-saturated specimen formed under lower pore pressure is higher than that of specimens formed under higher pore pressure, even when measured with identical effective stresses.

[46] 5. The stiffness and failure strength of gas-saturated specimens are higher than those of water-saturated specimens. The gas-saturated specimens show an apparent strain-softening behavior which is noticeably different from that of water-saturated specimens. The volumetric strain of gas-saturated specimens is larger than that of water-saturated specimens and showed a positive dilation.

[47] These findings are expected to be used to fully understand the deformation behavior of methane hydrate-bearing sediments and to establish a constitutive model in future studies. During the production of methane hydrate reservoirs, hydrate will convert to gas plus water. The sediments are neither gas-saturated nor water-saturated; they always are partially water-saturated. The pore fluid significantly affects on the hydromechanical behavior of hydrate-bearing sediments as shown in our study. It is essential to investigate the mechanical properties of partially water-saturated methane hydrate-bearing sediments in further studies.

[48] **Acknowledgments.** This work was supported by a grant-in aid for scientific research (A) 20246080 from the Japan Society for the Promotion of Science. The second author was supported to stay in Yamaguchi University as a research student by a grant from the Major National S&T Program (2011ZX05026-004) and a scholarship under the State Scholarship Fund of China Scholarship Council. The authors would like to express their sincere thanks to their supporters. The authors also thank associate editor and referees (W. Waite) for their helpful comments.

## References

- Boswell, R. (2009), Is gas hydrate energy within reach?, *Science*, 325(5943), 957–958, doi:10.1126/science.1175074.
- Boswell, R., and T. S. Collett (2011), Current perspectives on gas hydrate resources, *Energ. Environ. Sci.*, 4(4), 1206–1215, doi:10.1039/c0ee00203h.
- Brown, H. E., W. S. Holbrook, M. J. Hornbach, and J. Nealon (2006), Slide structure and role of gas hydrate at the northern boundary of the Storegga Slide, offshore Norway, *Mar. Geol.*, 229(3–4), 179–186, doi:10.1016/j.margeo.2006.03.011.
- Circone, S., S. H. Kirby, and L. A. Stern (2005), Direct measurement of methane hydrate composition along the hydrate equilibrium boundary, *J. Phys. Chem. B*, 109(19), 9468–9475, doi:10.1021/jp0504874.
- Collett, T. S., M. W. Lee, W. F. Agena, J. J. Miller, K. A. Lewis, M. V. Zyrianova, R. Boswell, and T. L. Inks (2011), Permafrost-associated natural gas hydrate occurrences on the Alaska North Slope, *Mar. Petrol. Geol.*, 28(2), 279–294, doi:10.1016/j.marpetgeo.2009.12.001.
- Dawe, R. A., and S. Thomas (2007), A large potential methane source—Natural gas hydrates, *Energ. Source Part A*, 29(3), 217–229, doi:10.1080/009083190948676.
- Durham, W. B., S. H. Kirby, L. A. Stern, and W. Zhang (2003), The strength and rheology of methane clathrate hydrate, *J. Geophys. Res.*, 108(B4), 2182, doi:10.1029/2002JB001872.
- Ebinuma, T., Y. Kamata, H. Minagawa, R. Ohmura, J. Nagao, and H. Narita (2005), Mechanical properties of sandy sediment containing methane hydrate, paper presented at *Proceedings of the 5th International Conference on Gas Hydrates (ICGH2005)*, Trondheim, Norway.
- Glasby, G. P. (2003), Potential impact on climate of the exploitation of methane hydrate deposits offshore, *Mar. Petrol. Geol.*, 20(2), 163–175, doi:10.1016/S0264-8172(03)00021-7.
- Graham, J., M. Alfaro, and G. Ferris (2004), Compression and strength of dense sand at high pressures and elevated temperatures, *Can. Geotech. J.*, 41(6), 1206–1212, doi:10.1139/T04-047.
- Guerin, G., D. Goldberg, and A. Meltser (1999), Characterization of in situ elastic properties of gas hydrate-bearing sediments on the Blake Ridge, *J. Geophys. Res.*, 104(B8), 17,781–17,795, doi:10.1029/1999JB900127.
- Helgerud, M. B., W. F. Waite, S. H. Kirby, and A. Nur (2009), Elastic wave speeds and moduli in polycrystalline ice Ih, sl methane hydrate, and sII methane-ethane hydrate, *J. Geophys. Res.*, 114, B02212, doi:10.1029/2008JB006132.
- Hyodo, M., Y. Nakata, N. Yoshimoto, and T. Ebinuma (2005), Basic research on the mechanical behavior of methane hydrate-sediments mixture, *Soils found.*, 45(1), 75–85.
- Hyodo, M., J. Yoneda, Y. Nakata, and N. Yoshimoto (2011), Strength and dissociation property of methane hydrate bearing sand, paper presented at *Proceedings of the 7th International Conference on Gas Hydrates (ICGH 2011)*, Edinburgh, Scotland, U. K.
- Hyodo, M., J. Yoneda, N. Yoshimoto, and Y. Nakata (2013), Mechanical and dissociation properties of methane hydrate-bearing sand in deep seabed, *Soils Found.*, 53(2), 299–314, doi:10.1016/j.sandf.2013.02.010.
- Lee, J. Y., T. S. Yun, J. C. Santamarina, and C. Ruppel (2007), Observations related to tetrahydrofuran and methane hydrates for laboratory studies of hydrate-bearing sediments, *Geochem., Geophys., Geosyst.*, 8, Q6003, doi:10.1029/2006GC001531.
- Li, Y., Y. Song, F. Yu, W. Liu, and J. Zhao (2011), Experimental study on mechanical properties of gas hydrate-bearing sediments using kaolin clay, *China Ocean Eng.*, 25(1), 113–122, doi:10.1007/s13344-011-0009-6.
- Li, Y., Y. Song, W. Liu, F. Yu, R. Wang, and X. Nie (2012a), Analysis of mechanical properties and strength criteria of methane hydrate-bearing sediments, *Int. J. Offshore Polar*, 22(4), 290–296.
- Li, Y., Y. Song, W. Liu, and F. Yu (2012b), Experimental research on the mechanical properties of methane hydrate-ice mixtures, *Energies*, 5(2), 181–192, doi:10.3390/en5020181.
- Li, Y., H. Zhao, F. Yu, Y. Song, W. Liu, Q. Li, and H. Yao (2012c), Investigation of the stress-strain and strength behavior of ice containing methane hydrate, *J. Cold Reg. Eng.*, 26(4), 149–159, doi:10.1061/(ASCE)CR.1943-5495.0000044.
- Li, Y., Y. Song, W. Liu, F. Yu, and R. Wang (2013), A new strength criterion and constitutive model of gas hydrate-bearing sediments under high confining pressures, *J. Petrol. Sci. Eng.*, 109, 45–50, doi:10.1016/j.petrol.2013.08.010.
- Masui, A., H. Haneda, Y. Ogata, and K. Aoki (2005), The effect of saturation degree of methane hydrate on the shear strength of synthetic methane hydrate sediments, paper presented at *Proceedings of the 5th International Conference on Gas Hydrates (ICGH 2005)*, Trondheim, Norway.
- Masui, A., K. Miyazaki, H. Haneda, Y. Ogata, and K. Aoki (2008), Mechanical characteristics of natural and artificial gas hydrate bearing sediments, paper presented at *Proceedings of the 6th International Conference on Gas Hydrates (ICGH 2008)*, Vancouver, British Columbia, Canada.
- Milkov, A. V. (2004), Global estimates of hydrate-bound gas in marine sediments: How much is really out there?, *Earth Sci. Rev.*, 66(3–4), 183–197, doi:10.1016/j.earscirev.2003.11.002.
- Miyazaki, K., A. Masui, Y. Sakamoto, K. Aoki, N. Tenma, and T. Yamaguchi (2011), Triaxial compressive properties of artificial methane-hydrate-bearing sediment, *J. Geophys. Res.*, 116, B06102, doi:10.1029/2010JB008049.
- Ning, F., Y. Yu, S. Kjelstrup, T. J. H. Vlught, and K. Glavatskiy (2012), Mechanical properties of clathrate hydrates: Status and perspectives, *Energ. Environ. Sci.*, 5(5), 6779–6795, doi:10.1039/c2ee03435b.
- Priest, J. A., E. V. L. Rees, and C. R. I. Clayton (2009), Influence of gas hydrate morphology on the seismic velocities of sands, *J. Geophys. Res.*, 114, B11205, doi:10.1029/2009JB006284.
- Rutqvist, J., G. J. Moridis, T. Grover, and T. Collett (2009), Geomechanical response of permafrost-associated hydrate deposits to depressurization-induced gas production, *J. Petrol. Sci. Eng.*, 67(1–2), 1–12, doi:10.1016/j.petrol.2009.02.013.
- Sloan, E. D. (1998), Gas hydrates: Review of physical/chemical properties, *Energ. Fuel*, 12(2), 191–196, doi:10.1021/ef970164+.
- Sloan, E. D. (2003), Fundamental principles and applications of natural gas hydrates, *Nature*, 426(6964), 353–359, doi:10.1038/nature02135.
- Suzuki, K., T. Ebinuma, and H. Narita (2009), Features of methane hydrate-bearing sandy-sediments of the forearc basin along the Nankai trough: Effect on methane hydrate-accumulating mechanism in turbidite, *J. Geol.*, 118(5), 899–912, doi:10.5026/jgeography.118.899.
- Uchida, S., K. Soga, and K. Yamamoto (2012), Critical state soil constitutive model for methane hydrate soil, *J. Geophys. Res.*, 117, B03209, doi:10.1029/2011JB008661.
- Waite, W. F., W. J. Winters, and D. H. Mason (2004), Methane hydrate formation in partially water-saturated Ottawa sand, *Am. Mineral.*, 89(8–9), 1202–1207.
- Waite, W. F., T. J. Kneafsey, W. J. Winters, and D. H. Mason (2008), Physical property changes in hydrate-bearing sediment due to depressurization and

- subsequent repressurization, *J. Geophys. Res.*, *113*, B07102, doi:10.1029/2007JB005351.
- Waite, W. F., et al. (2009), Physical properties of gas hydrate-bearing sediments, *Rev. Geophys.*, *47*, RG4003, doi:10.1029/2008RG000279.
- Yang, S., D. M. Kleehammer, Z. Huo, E. D. Sloan, and K. T. Miller (2004), Temperature dependence of particle-particle adherence forces in ice and clathrate hydrates, *J. Colloid Interf. Sci.*, *277*(2), 335–341, doi:10.1016/j.jcis.2004.04.049.
- Yoneda, J., M. Hyodo, Y. Nakata, and N. Yoshimoto (2008), Time-dependent elasto-plastic constitutive equation for sedimentary sands supported by methane hydrate, paper presented at *Proceedings of the 12th Japan Symposium on Rock Mechanics*, Ube, Japan.
- Yoneda, J., M. Hyodo, Y. Nakata, N. Yoshimoto, Y. Imamura, and N. Tenma (2011), Localized deformation of methane hydrate-bearing sand by plane strain shear tests, paper presented at *Proceedings of the 7th International Conference on Gas Hydrates (ICGH 2011)*, Edinburgh, Scotland, U. K.
- Yuan, T., G. D. Spence, R. D. Hyndman, T. A. Minshull, and S. C. Singh (1999), Seismic velocity studies of a gas hydrate bottom-simulating reflector on the northern Cascadia continental margin: Amplitude modeling and full waveform inversion, *J. Geophys. Res.*, *104*(B1), 1179–1191, doi:10.1029/1998JB900020.
- Yun, T. S., J. C. Santamarina, and C. Ruppel (2007), Mechanical properties of sand, silt, and clay containing tetrahydrofuran hydrate, *J. Geophys. Res.*, *112*, B04106, doi:10.1029/2006JB004484.